Research Article | Vol. 31, No. 21 / 9 Oct 2023 / Optics Express 34626
Optics EXPRESS

Integrated density of states algorithm for one-dimensional randomly layered optical media

GLEN J. KISSEL*

Department of Engineering, University of Southern Indiana, 8600 University Blvd., Evansville, IN 47712, USA
*gkissel@usi.edu

Abstract: Anderson localization simulations in one-dimensional disordered optical systems usually focus on the localization length or its inverse, but the calculation of the density of states has appeared less frequently for such models. In this paper a technique originally used to calculate the integrated density of states for one-dimensional disordered crystals supporting electron propagation is modified for use with randomly layered optical media. The density of states is then readily available via differentiation. The algorithm is demonstrated on one-dimensional quarter-wave stack and non-quarter-wave stack models with layer thicknesses disordered.

1. Introduction

The study of Anderson localization in one-dimensional (1D) optical systems has continued apace for over three decades [1–20], with a strong focus on calculating the localization length or its inverse. Density of states (DOS) simulations for disordered 1D optical systems have appeared less frequently. This is likely explained by the ease with which the localization length can be calculated, namely by tracking the growth of a state vector or state ratio to calculate a Lyapunov exponent then taking the reciprocal. By contrast, the DOS is arrived at via differentiation of the integrated density of states (IDOS), which itself depends on a phase calculation, and ideally a nonreduced phase calculation, and thus presents much more of a computational challenge than the localization length. In addition the localization length adequately captures the key effect of Anderson localization, while the DOS's connection with the Lyapunov exponent (inverse localization length on a per bay basis) is seemingly mathematically obscured via the Herbert-Jones-Thouless formula [9,19].

In the literature DOS calculations have been confined to simulations of a system with a single passband [6,9] or to simulation of a single bandgap of a multi-bandgap system [5]. In these instances eigenvalues were extracted from a transfer matrix with the model limited to the simulation of hundreds of cells. Excellent analytical work [7] was done following up [5], but this was based on a reduced phase and a reduced IDOS after which stringent approximations were imposed with results displayed over only part of a bandgap and a bit beyond. A disordered 1D photonic crystal with sinusoidally varying index of refraction was considered in [17], but the IDOS was shown for only one bandgap. A synthetic photonic lattice disordered temporally [18] simulated DOS for 10^5 temporal cells, but was limited to two symmetric bands separated by a gap, and, in addition, the DOS calculation technique was not explained. In contrast, this paper provides a numerical algorithm for the IDOS applicable to a disordered 1D multi-passband layered optical system with an almost limitless number of cells.

A technique not sufficiently appreciated to calculate the IDOS, with DOS being available via differentiation, was originally developed by Lax and Phillips [21], then modified by Makinson and Roberts [22], for electron propagation in 1D disordered crystals. This latter modification is the jumping off point for the present paper. Their technique is modified for layered optical

#502330 https://doi.org/10.1364/OE.502330
Journal © 2023 Received 1 Aug 2023; revised 14 Sep 2023; accepted 21 Sep 2023; published 29 Sep 2023

Optics EXPRESS

media in which layer thicknesses or indices of refraction or both could be randomized allowing simulation of IDOS and DOS over multiple passbands and bandgaps.

Section 2 of this paper will describe the algorithm to calculate the IDOS based on the work of [22]. This is followed in Section 3 by simulation results of both the IDOS and DOS for quarter-wave stack and non-quarter-wave stack models from [23] with layer thicknesses randomized. Concluding remarks are made in Section 4.

2. Algorithm to calculate integrated density of states for 1D randomly layered optical media

To fix ideas and clarify notation we first examine the 1D periodic optical waveguide model of [12] which consists of the repetition of two successive layers of thicknesses l_1 and l_2, with corresponding piecewise constant indices of refraction n_1 and n_2, with layer thicknesses later randomized in this paper. Two layers constitute a cell. The transfer through the two layers of the ith cell is executed in two steps:

$$\begin{bmatrix} \psi \\ \psi' \end{bmatrix}_i^{(1)} = \begin{bmatrix} \cos(n_1 l_1 k_0) & \dfrac{\sin(n_1 l_1 k_0)}{n_1 k_0} \\ -n_1 k_0 \sin(n_1 l_1 k_0) & \cos(n_1 l_1 k_0) \end{bmatrix} \begin{bmatrix} \psi \\ \psi' \end{bmatrix}_{i-1}^{(2)} \tag{1}$$

$$\begin{bmatrix} \psi \\ \psi' \end{bmatrix}_i^{(2)} = \begin{bmatrix} \cos(n_2 l_2 k_0) & \dfrac{\sin(n_2 l_2 k_0)}{n_2 k_0} \\ -n_2 k_0 \sin(n_2 l_2 k_0) & \cos(n_2 l_2 k_0) \end{bmatrix} \begin{bmatrix} \psi \\ \psi' \end{bmatrix}_i^{(1)} \tag{2}$$

where $\psi = \psi(x,\ \bar{\omega})$ is the Cartesian component of the electric field at normal incidence, with x the space variable in the direction of repetition, $\bar{\omega}$ is a non-dimensional frequency to be specified later, ψ' is the first partial derivative with respect to the space variable, and k_0 is the propagation number in vacuum. Also note the use of the superscripts in the equations above and below. The superscript (1) means $\lim x \to l_1 - 0$, the edge of layer l_1 just before layer l_2, and similarly superscript (2) means $\lim x \to l_2 - 0$, the edge of layer l_2 just before layer l_1.

The goal of the algorithm is to find $I(\bar{\omega})$ the number of eigenstates less than some frequency $\bar{\omega}$, normalized by the number of cells N, namely, the IDOS for positive frequencies $I(\bar{\omega}) = \int_0^{\bar{\omega}} \rho(\tilde{\bar{\omega}}) d\tilde{\bar{\omega}}$, where the DOS $\rho(\bar{\omega}) = \sum_j \delta(\bar{\omega} - \bar{\omega}_j)/N$. With appropriate boundary conditions it is well known [22,24] that $NI(\bar{\omega})$ is the number of nodes of ψ and so the IDOS is readily available via a node count of ψ. Further [21] clarifies that computations of the node count are simplified by tracking the sign changes of the state ratio ψ'/ψ. Also see the extensive discussion of [25], though note his use of the reciprocal ratio, ψ/ψ'. The question is how to properly execute that count over multiple passbands. We find that the algorithm of [22] properly executes the count for a Kronig-Penney type model, and so given the mathematical correspondence noted by [23] between the Kronig-Penney model and one-dimensional optical layered systems this suggests appropriate modifications of the algorithm of [22] should work for our purposes.

Continuing from Eq. (1) we have,

$$\psi_i'^{(1)} = -n_1 k_0 \sin(n_1 l_1 k_0) \psi_{i-1}^{(2)} + \cos(n_1 l_1 k_0) \psi_{i-1}'^{(2)} \tag{3}$$

and

$$\psi_i^{(1)} = \cos(n_1 l_1 k_0) \psi_{i-1}^{(2)} + \frac{\sin(n_1 l_1 k_0)}{n_1 k_0} \psi_{i-1}'^{(2)}. \tag{4}$$

Rewriting Eq. (4)

$$n_1 k_0 \psi_i^{(1)} = \cos(n_1 l_1 k_0) n_1 k_0 \psi_{i-1}^{(2)} + \sin(n_1 l_1 k_0) \psi_{i-1}'^{(2)} \tag{5}$$

Optics EXPRESS

then taking the ratio of Eqs. (3) and (5) we arrive at an equation for the (normalized) state ratio for this layer on which we will do the node count leading to the IDOS:

$$\left(\frac{\psi'}{n_1 k_0 \psi}\right)_i^{(1)} = \frac{-n_1 k_0 \sin(n_1 l_1 k_0)\,\psi_{i-1}^{(2)} + \cos(n_1 l_1 k_0)\,\psi_{i-1}'^{(2)}}{\cos(n_1 l_1 k_0)\,n_1 k_0 \psi_{i-1}^{(2)} + \sin(n_1 l_1 k_0)\,\psi_{i-1}'^{(2)}}. \tag{6}$$

Further simplification of the right side of Eq. (6) leads to

$$\left(\frac{\psi'}{n_1 k_0 \psi}\right)_i^{(1)} = \frac{\frac{-n_1 k_0 \sin(n_1 l_1 k_0)\psi_{i-1}^{(2)}}{\cos(n_1 l_1 k_0) n_1 k_0 \psi_{i-1}^{(2)}} + \frac{\cos(n_1 l_1 k_0)\psi_{i-1}'^{(2)}}{\cos(n_1 l_1 k_0) n_1 k_0 \psi_{i-1}^{(2)}}}{1 + \frac{\sin(n_1 l_1 k_0)\psi_{i-1}'^{(2)}}{\cos(n_1 l_1 k_0) n_1 k_0 \psi_{i-1}^{(2)}}}. \tag{7}$$

This reduces to

$$\left(\frac{\psi'}{n_1 k_0 \psi}\right)_i^{(1)} = \frac{\frac{\psi_{i-1}'^{(2)}}{n_1 k_0 \psi_{i-1}^{(2)}} - \tan(n_1 l_1 k_0)}{1 + \tan(n_1 l_1 k_0)\,\frac{\psi_{i-1}'^{(2)}}{n_1 k_0 \psi_{i-1}^{(2)}}}. \tag{8}$$

Now letting $-\tan\phi_{i-1\to i}^{(2\to 1)} = \frac{\psi_{i-1}'^{(2)}}{n_1 k_0 \psi_{i-1}^{(2)}}$ and $-\tan\chi_i^{(1)} = \left(\frac{\psi'}{n_1 k_0 \psi}\right)_i^{(1)}$ in Eq. (8), and multiplying both sides of the resulting equation by (-1), we arrive at:

$$\tan\chi_i^{(1)} = \frac{\tan\phi_{i-1\to i}^{(2\to 1)} + \tan(n_1 l_1 k_0)}{1 - \tan\phi_{i-1\to i}^{(2\to 1)}\tan(n_1 l_1 k_0)}. \tag{9}$$

Note the use of the superscript (2→1) which means the $\lim x \to l_2 + 0$ indicating the transition from layer l_2 to the beginning of layer l_1 and similarly the subscript $i-1 \to i$ indicating the transition to the ith cell. Invoking a trigonometric identity, we have

$$\tan\chi_i^{(1)} = \tan(\phi_{i-1\to i}^{(2\to 1)} + n_1 l_1 k_0). \tag{10}$$

And finally,

$$\chi_i^{(1)} = \phi_{i-1\to i}^{(2\to 1)} + n_1 l_1 k_0. \tag{11}$$

A similar line of reasoning can be executed for layer l_2 of the ith cell resulting in

$$\chi_i^{(2)} = \phi_i^{(1\to 2)} + n_2 l_2 k_0 \tag{12}$$

where the superscript (1→2) means the $\lim x \to l_1 + 0$ indicating the transition from layer l_1 to the beginning of layer l_2.

With these mathematical preliminaries out of the way, we are now in a position to set out the algorithm to do the node counting. The algorithm will carefully take into account the two layers making up each cell and, crucially, the transition between the two layers. First we set out some simplifying notation, letting

$$a_i^{(1)} = -\tan\chi_i^{(1)} \tag{13}$$

$$b_i^{(1\to 2)} = -\tan\phi_i^{(1\to 2)} \tag{14}$$

$$a_i^{(2)} = -\tan\chi_i^{(2)} \tag{15}$$

$$b_{i-1\to i}^{(2\to 1)} = -\tan\phi_{i-1\to i}^{(2\to 1)}. \tag{16}$$

First, initializations are set with $idossum_0^{(2)} = 0$, whose subsequent terms will accumulate the node count as the algorithm proceeds thru the bilayers of each cell, and $a_0^{(2)} = 1$, and with

Optics EXPRESS

$-\frac{\pi}{2} \le \phi_{i-1\to i}^{(2\to 1)} \le \frac{\pi}{2}$, and $-\frac{\pi}{2} \le \phi_i^{(1\to 2)} \le \frac{\pi}{2}$, the algorithm proceeds by immediately transitioning to layer l_1 with refractive index n_1 of cell $i = 1$,

$$b_{i-1\to i}^{(2\to 1)} = \frac{n_2}{n_1} a_{i-1}^{(2)} \tag{17}$$

$$\phi_{i-1\to i}^{(2\to 1)} = \tan^{-1}(-b_{i-1\to i}^{(2\to 1)}) \tag{18}$$

$$\chi_i^{(1)} = \phi_{i-1\to i}^{(2\to 1)} + n_1 l_1 k_0 \tag{19}$$

$$idossum_i^{(1)} = \text{int}\left[\left(\chi_i^{(1)} + \frac{\pi}{2}\right)/\pi\right] + idossum_{i-1}^{(2)} \tag{20}$$

where int [] takes the integer part of the argument; the algorithm continues,

$$a_i^{(1)} = -\tan \chi_i^{(1)} \tag{21}$$

now the transition is made to layer l_2 with refractive index n_2

$$b_i^{(1\to 2)} = \frac{n_1}{n_2} a_i^{(1)} \tag{22}$$

$$\phi_i^{(1\to 2)} = \tan^{-1}(-b_i^{(1\to 2)}) \tag{23}$$

$$\chi_i^{(2)} = \phi_i^{(1\to 2)} + n_2 l_2 k_0 \tag{24}$$

$$idossum_i^{(2)} = \text{int}\left[\left(\chi_i^{(2)} + \frac{\pi}{2}\right)/\pi\right] + idossum_i^{(1)} \tag{25}$$

$$a_i^{(2)} = -\tan \chi_i^{(2)} \tag{26}$$

with the algorithm continuing into the next cell, i.e., into the next double layer via Eq. (17). After iterating through all of the cells the IDOS is calculated as

$$I(\bar{\omega}) = \frac{idossum_N^{(2)}}{N} \,. \tag{27}$$

Because there is no final boundary condition imposed for the algorithm there is a ±1 ambiguity in the node count. The DOS is then found by numerical differentiation, namely $\rho(\bar{\omega}) = \frac{dI(\bar{\omega})}{d\bar{\omega}}$

An explanation is warranted of the argument of the int[] and of the $\phi_{i-1\to i}^{(2\to 1)}$ and $\phi_i^{(1\to 2)}$ terms, which we will refer to collectively as ϕ_i, and likewise χ_i for $\chi_i^{(1)}$ and $\chi_i^{(2)}$. In Eqs. (20) and (25) the int[] function truncates the phase in order to properly update the node count $(idossum_i^{(1,2)})$ with the proper integer number of nodes in a given layer. But the phase remainder, which ranges between 0 and π, cannot simply be discarded. That phase remainder is carried forward with the tan χ_i function, then scaled and followed by an arctan giving ϕ_i which now carries the phase remainder into the next layer. But this process with the tan and arctan operations causes the phase remainder, ϕ_i, to now range from $-\frac{\pi}{2}$ to $+\frac{\pi}{2}$. Therefore in Eqs. (20) and (25) a phase of $\frac{\pi}{2}$ has to be added back. In this way the phase is properly accounted for in the algorithm.

3. Quarter-wave stack and non-quarter-wave stack simulations

The parameters in Eqs. (1) and (2) were set to the quarter-wave stack (QWS) and non-quarter-wave stack models (Non-QWS) described in [23], after which layer thicknesses were randomized and the above algorithm employed to calculate the IDOS and DOS for those models. Extensive simulations show that the IDOS and DOS are self-averaging quantities, so Monte Carlo results below are done for very long stacks ($N = 10^6$ or 10^8) without any ensemble averaging. For the

Optics EXPRESS

worst case, namely the DOS of the Non-QWS at 10% disorder for frequencies just above the sixth bandgap, the result is stable to the second rounded decimal for a simulation with 10^8 cells, and such stability will suffice for our purposes.

Following [23] we let $n_1 = 1.45$ and $n_2 = 2.65$ for both models and calculate results for non-dimensional frequency $\bar{\omega} = \omega(l_1 + l_2)/c = \omega\Lambda/c$ over the range of 0 to 10, which spans the IR through the UV. Note that $k_0 = \bar{\omega}/\Lambda$. In what follows the IDOS and DOS for the perfectly periodic models (blue line in the figures) were generated from the unwrapped Bloch wavefunction, $K = K(\bar{\omega})$ (a reduced band structure is presented in [23] as $\bar{\omega}$ versus $K\Lambda$), where $I(\bar{\omega})_{periodic} = \frac{|Re(K\Lambda)|}{\pi}$ and $\rho(\bar{\omega})_{periodic} = \frac{d|Re(K\Lambda)|}{\pi d\bar{\omega}}$.

3.1. Quarter-wave stack

For the QWS simulations $l_1 = \lambda_0/4n_1 = 258.6\ nm$, $l_2 = \lambda_0/4n_2 = 141.5\ nm$, with $\lambda_0 = 1.5\ \mu m$. The results for the perfectly periodic model were generated, then the two randomized models were produced by drawing each layer thickness l_1 and l_2 from uniform probability density functions of width $[l_{1,2} \pm \Delta l_{1,2}]$ where $\Delta = 0.05$, then $\Delta = 0.1$, i.e. 5% and 10% disorder, thus each layer was simultaneously randomized in the same manner.

The results for the IDOS of the QWS are shown across the full frequency range in Fig. 1. The existence in the QWS of two vanished even photonic bandgaps, one between the first and second bandgaps and another between the second and third bandgaps, results in a value of three and five, respectively, for the second and third bandgaps of the IDOS. Note as frequency ranges through the first passband and bandgap to higher passbands and bandgaps, the algorithm provides a continuous function, and as disorder increases, the edges of the higher bandgaps are substantially smoothed.

The IDOS of the QWS is shown in close-up fashion for its third bandgap in Fig. 2. With 5% disorder in the layer thicknesses the bandgap is reduced by close to 50% of its perfectly periodic width, and then is completely obliterated with disorder at the 10% level.

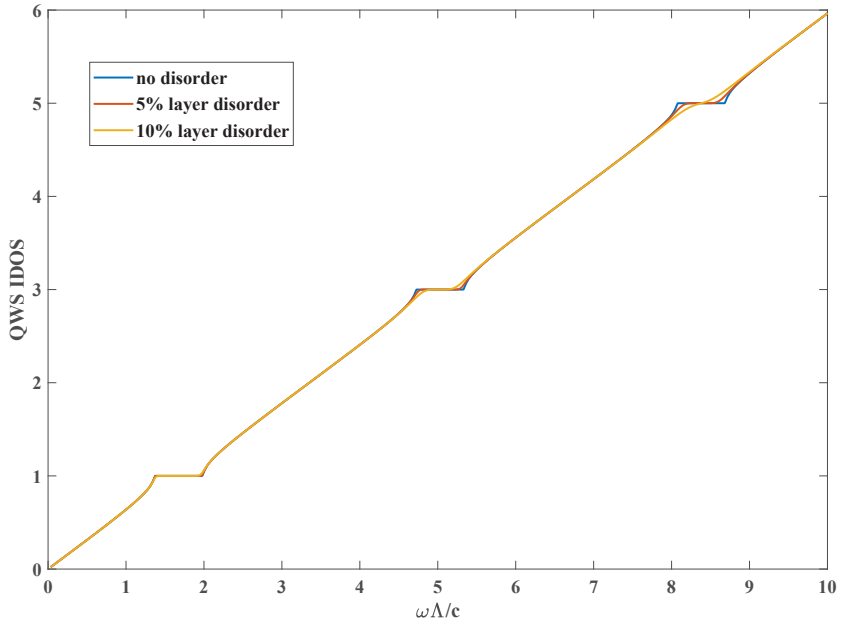

Fig. 1. IDOS for perfectly periodic QWS and two randomized QWS models with each bilayer thickness randomized 5% and 10%, using 10^6 cells in the randomized simulations.

Optics EXPRESS

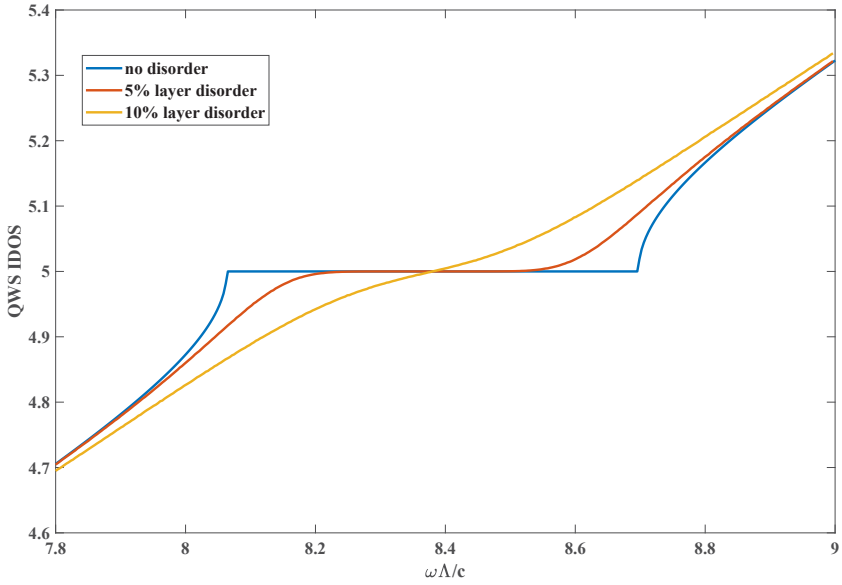

Fig. 2. IDOS for third bandgap of perfectly periodic QWS and two randomized stacks with each bilayer thickness randomized 5% and 10%, using 10^6 cells in the randomized simulations.

The DOS, calculated via numerical differentiation of the corresponding IDOS results, are shown for the perfectly periodic QWS model and the two disordered models in Fig. 3.

Clearly these levels of disorder had little impact on the first bandgap, while the second bandgap begins suffering a decrease in its frequency range at 5% disorder and becomes quite narrow at 10% disorder, and finally in the third bandgap the 5% disorder substantially narrows the third

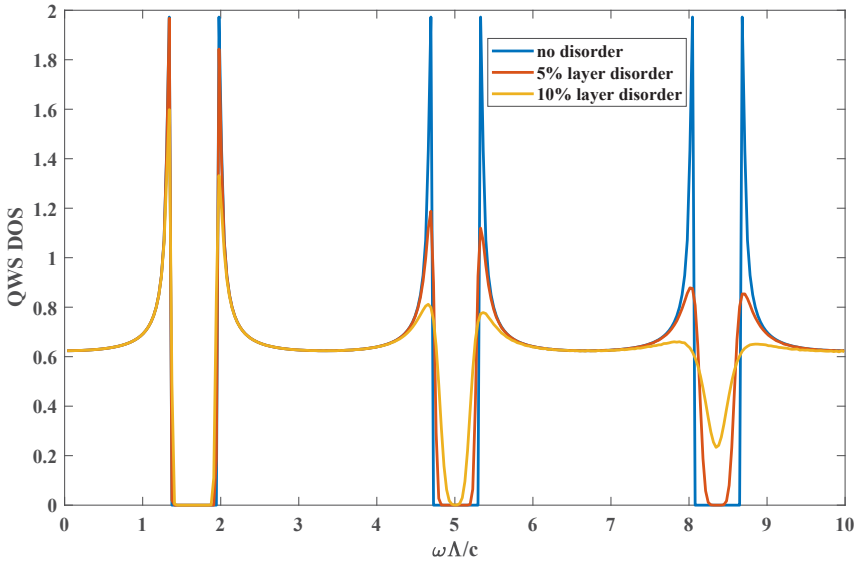

Fig. 3. DOS for perfectly periodic QWS and two randomized stacks with each bilayer thickness randomized 5% and 10%, using 10^8 cells in the randomized simulations.

Optics EXPRESS

bandgap while the 10% disorder wipes out the third bandgap entirely. In addition, the bandedge peaks became more rounded with increasing frequency and increasing disorder.

Finally, it should be noted that for the QWS a singularity appeared in the middle of the first and third bandgap of the IDOS and DOS for this algorithm when the disorder was set exactly to zero. The singularities could no longer be discerned, for example, when just a small amount of disorder ($\Delta = 10^{-10}$) was included for simulations of $N \geq 10^5$ cells. This is displayed in Fig. 4. Otherwise, there was a perfect match between the $I(\bar{\omega})_{periodic}$ and $\rho(\bar{\omega})_{periodic}$ and their counterparts generated by this algorithm.

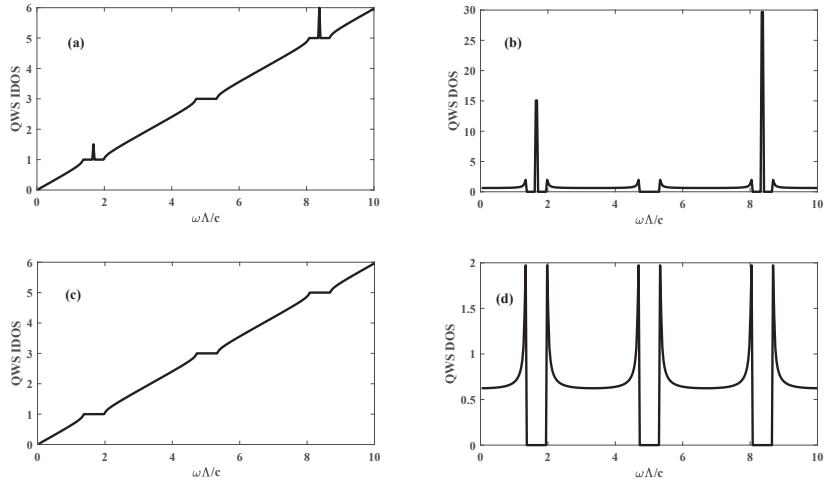

Fig. 4. IDOS for perfectly periodic QWS ($\Delta = 0$) in (a) showing the singularities in the middle of the first and third bandgaps with corresponding DOS in (b), and in (c) the IDOS for the very slightly randomized QWS model ($\Delta = 10^{-10}$) with corresponding DOS in (d) using 10^6 cells in each simulation.

3.2. Non-quarter-wave stack

To further exercise the algorithm, a Non-QWS counterpart to the QWS model in the previous section was employed. From [23] the Non-QWS has layer thicknesses $l_1 = 200.05$ *nm*, and $l_2 = 200.05$ *nm* which are then subjected to randomization. This Non-QWS has a much richer bandgap structure with six bandgaps over the same frequency range for which there were only three bandgaps in the QWS counterpart. In particular the third bandgap of the Non-QWS is very narrow.

The results for the IDOS of the Non-QWS are shown across the full frequency range in Fig. 5. Again, note as frequency ranges through the first passband and bandgap to higher passbands and bandgaps, the algorithm provides a continuous function, and as disorder increases, the edges of the higher bandgaps are increasingly smoothed as in the QWS counterpart. Note the six bandgaps across the frequency range.

We display the close-up IDOS results for the sixth bandgap in Fig. 6, but in this case limiting the disorder first to 2.5% resulting in a close to 50% reduction in the bandgap, and then to 5% disorder obliterating the bandgap completely.

The DOS found via numerical differentiation of the IDOS results are presented for this Non-QWS in Fig. 7 for 5% and 10% layer disorders, as well as for the perfectly periodic case.

Clearly, the disorder produced increasingly narrow or even vanishing bandgaps as frequency increased, though the very narrow third bandgap has suffered this more intensely despite being in the middle of the frequency range. Again, bandedge peaks were eroded with increasing

Optics EXPRESS

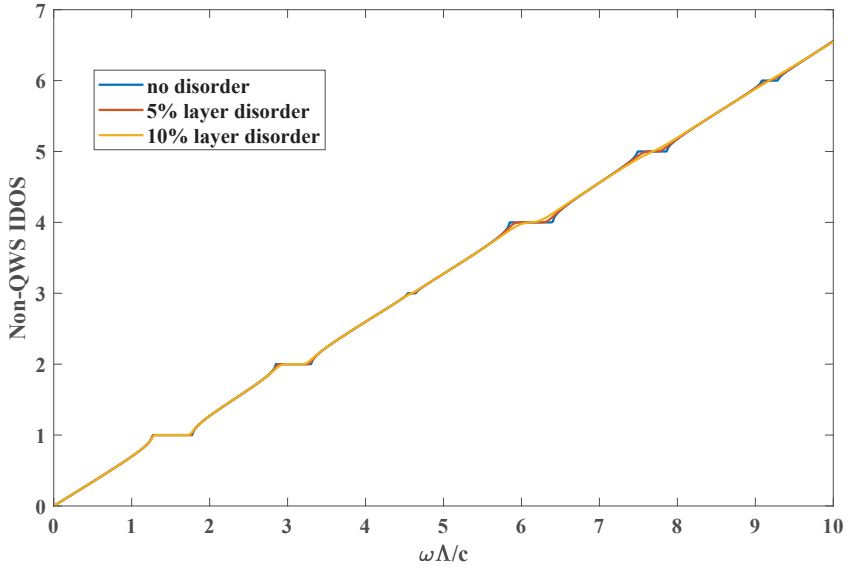

Fig. 5. IDOS for perfectly periodic Non-QWS and two randomized Non-QWS models with each bilayer thickness randomized 5% and 10%, using 10^6 cells in the randomized simulations.

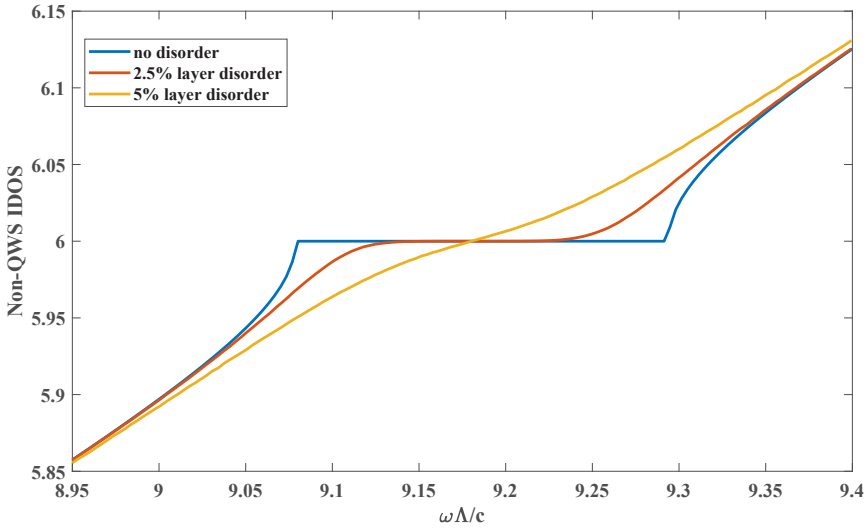

Fig. 6. IDOS for sixth bandgap of perfectly periodic Non-QWS model and two models with each bilayer thickness randomized 2.5% and 5%, using 10^6 cells in the randomized simulations.

frequency and disorder, though the third bandgap edges suffered more than those of the next higher frequency bandedge. The difference in narrowing or obliterating of bandgaps in going from 5% disorder to 10% disorder is most obvious in the second, fourth and fifth bandgaps, with the second bandgap narrowed and the fourth and fifth bandgaps obliterated. Otherwise the first bandgap is not much affected by the jump from 5% to 10% disorder, while the third and sixth bandgaps had already disappeared at 5% disorder and simply had a larger DOS value at 10% disorder. No singularities were noted in the algorithm as the disorder went to zero for this model,

Optics EXPRESS

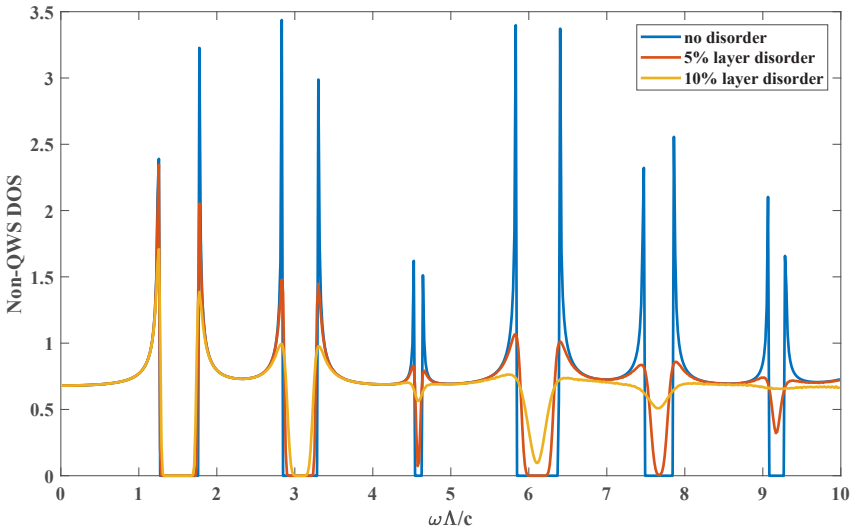

Fig. 7. DOS for perfectly periodic Non-QWS and for models with each bilayer thickness randomized 5% then 10%, using 10^8 cells in the randomized simulations.

and the zero-disorder model coincided precisely with the $I(\bar{\omega})_{periodic}$ and $\rho(\bar{\omega})_{periodic}$ generated from the Non-QWS band structure.

4. Conclusion

A numerical algorithm capable of determining the IDOS, and DOS via differentiation, across multiple bandgaps for 1D layered optical media has been demonstrated on QWS and Non-QWS models with layer thicknesses randomized. A singularity in the IDOS/DOS was noted for the middle of two bandgaps of only the QWS when the disorder went to zero in the algorithm, and the singularity was not discernible for slightly nonzero disorder. The disorder most notably shrunk the highest frequency bandgaps, though the very narrow third bandgap near the middle of the frequency range of the Non-QWS was also noticeably impacted. Future papers will explore DOS calculations for models with randomized indices of refraction taking into account the Kramers-Kronig relations and for models with off-axis incidence and polarization effects. It is hoped this work will contribute to a more complete suite of numerical tools with which to study 1D optical Anderson localization.

Acknowledgments. The author is grateful to the University of Southern Indiana for computational resources.

Disclosures. The author declares no conflicts of interest.

Data availability. Data underlying the results presented in this paper are not publicly available at this time but may be obtained from the author upon reasonable request.

References

1. F. Bentosela and P. Piccoli, "An expression for attenuation in deformed optical waveguides," J. Phys. (Paris) **49**(12), 2001–2007 (1988).
2. A. Kondilis and P. Tzanetakis, "Numerical calculations on optical localization in multilayer structures with random-thickness layers," Phys. Rev. B **46**(23), 15426–15431 (1992).
3. J. M. Frigerio, J. Rivory, and P. Sheng, "Photonic bandtail in 1D randomly-perturbed periodic systems," Opt. Commun. **98**(4-6), 231–235 (1993).
4. O. Shapira and B. Fischer, "Localization of light in a random-grating array in a single-mode fiber," J. Opt. Soc. Am. B **22**(12), 2542–2552 (2005).

Optics EXPRESS

5. M. A. Kaliteevski, D. M. Beggs, S. Brand, R. A. Abram, and V. V. Nikolaev, "Statistics of the eigenmodes and optical properties of one-dimensional disordered photonic crystals," Phys. Rev. E **73**(5), 056616 (2006).
6. S. Mookherjea and A. Oh, "Effect of disorder on slow light velocity in optical slow-wave structures," Opt. Lett. **32**(3), 289–291 (2007).
7. A. A. Greshnov, M. A. Kaliteevski, R. A. Abram, S. Brand, and G. G. Zegrya, "Density of states in 1D disordered photonic crystals: Analytical solution," Solid State Commun. **146**(3-4), 157–160 (2008).
8. G. J. Kissel, "Ulam's method to estimate invariant measures and Lyapunov exponents for one-dimensional discretely randomized photonic structures," Proc. SPIE 7392, 73920S (2009).
9. S. Mookherjea, *Slow Light: Science and Applications*, J. B. Khurgin and R. S. Tucker, eds. (CRC, 2009), Chap. 7.
10. A. A. Asatryan, S. A. Gredeskul, L. C. Botten, M. A. Byrne, V. D. Freilikher, I. V. Shadrivov, R. C. McPhedran, and Y. S. Kivshar, "Anderson localization of classical waves in weakly scattering metamaterials," Phys. Rev. B **81**(7), 075124 (2010).
11. S. F. Liew and H. Cao, "Optical properties of 1D photonic crystals with correlated and uncorrelated disorder," J. Opt. **12**(2), 024011 (2010).
12. Y. Godin, S. Molchanov, and B. Vainberg, "The effect of disorder on the wave propagation in one-dimensional periodic optical systems," Waves Random Complex Media **21**(1), 135–150 (2011).
13. A. A. Asatryan, L. C. Botten, M. A. Byrne, V. D. Freilikher, S. A. Gredeskul, I. V. Shadrivov, R. C. McPhedran, and Y. S. Kivshar, "Transmission and Anderson localization in dispersive metamaterials," Phys. Rev. B **85**(4), 045122 (2012).
14. A. A. Greshnov, M. A. Kaliteevski, and R. A. Abram, "Analytical theory of light localization in one-dimensional disordered photonic crystals," Solid State Commun. **158**, 38–45 (2013).
15. A. Basiri, Y. Bromberg, A. Yamilov, H. Cao, and T. Kottos, "Light localization induced by a random imaginary refractive index," Phys. Rev. A **90**(4), 043815 (2014).
16. K. Kim, "Exact localization length for *s*-polarized electromagnetic waves incident at the critical angle on a randomly-stratified dielectric medium," Opt. Express **25**(23), 28752–28763 (2017).
17. R. A. Abram, A. A. Greshnov, S. Brand, and M. A. Kaliteevski, "A study of a phase formalism for calculating the cumulative density of states of one-dimensional photonic crystals," J. Mod. Opt. **64**(15), 1501–1509 (2017).
18. A. V. Pankov, I. D. Vatnik, D. V. Churkin, and S. A. Derevyanko, "Anderson localization in synthetic photonic lattice with random coupling," Opt. Express **27**(4), 4424–4434 (2019).
19. A. M. Merzlikin and R. S. Puzko, "Homogenization of Maxwell's equations in a layered system beyond the static approximation," Sci. Rep. **10**(1), 15783 (2020).
20. J. Niu, L. Du, F. Gao, and J. Zhao, "Modal analysis of transverse Anderson localization based on the imaginary distance BPM," Opt. Express **30**(24), 43900–43909 (2022).
21. M. Lax and J. C. Phillips, "One-dimensional impurity bands," Phys. Rev. **110**(1), 41–49 (1958).
22. R. E. B. Makinson and A. P. Roberts, "Zone theory of liquids," Aust. J. Phys. **13**(2), 437–445 (1960).
23. A. Yariv and P. Yeh, *Photonics: Optical Electronics in Modern Communications*, 6th ed. (Oxford, 2007), Chap. 12.
24. H. M. James and A. S. Ginzbarg, "Band structure in disordered alloys and impurity semiconductors," J. Phys. Chem. **57**(8), 840–848 (1953).
25. J. Hori, *Spectral Properties of Disordered Chains and Lattices* (Pergamon, 1968), Chap. 3.